Microstructure and Mechanical Properties of Semicrystalline−Rubbery−Semicrystalline Triblock Copolymers

Chong Min Koo,[†] Lifeng Wu,[†] Lisa S. Lim,[†] Mahesh K. Mahanthappa,[†] Marc A. Hillmyer,[‡] and Frank S. Bates*,[†]

Department of Chemical Engineering and Materials Science and Department of Chemistry, University of Minnesota, Minneapolis, Minnesota 55455

Received January 27, 2005; Revised Manuscript Received April 25, 2005

ABSTRACT: Microstructure of and mechanical properties of a series of symmetric EPE (E = poly(ethylene-*co*-1-butene) and P = poly(ethylene-*alt*-propylene)) triblock copolymers with M_n = 27−372 kg/mol have been investigated in the solid state. Microphase separation of EPE triblock copolymers originates from either (i) chemical incompatibility-induced microphase separation in the melt before crystallization at high overall molecular weights or (ii) crystallization-induced microphase separation from a homogeneous melt at low overall molecular weights. Small-angle X-ray scattering demonstrates that these EPEs ($f_E \approx f_P \approx 0.5$) adopt a lamellar morphology over the range of molecular weights studied. The observed interlamellar domain spacing (d) scales with the molecular weight as $d \sim N_0^{\beta}$, where N_0 is the degree of polymerization and $\beta = 0.22$ for crystallization-induced segregation and $\beta = 0.63$ for microphase-separated melts. The mode of microphase separation strongly affects the chain folding microstructure of the polyethylene crystallites within the lamellar structure. The consequences of these observations on the ultimate tensile strengths of these materials are discussed.

Introduction

Microphase separation and the resulting ordered structure formation in amorphous block copolymers have been extensively studied.[1−7] Diblock copolymers comprised of chemically incompatible blocks are known to adopt thermodynamic equilibrium morphologies such as spheres on a body-centered-cubic lattice, hexagonally packed cylinders, lamellae, and a bicontinuous network with *Ia*3*d* space-group symmetry depending on the chemical composition. The equilibrium structure formed by an A−B diblock copolymer depends on three parameters: χ, the Flory−Huggins interaction parameter between the incompatible blocks, N, the total number of segments in the block copolymer, and the volume fraction $f = f_A = 1 - f_B$. Mean-field theory calculations in the intermediate and strong segregation limits (moderate to large χN) demonstrate that symmetric diblock copolymers undergo microphase separation in the melt when $(\chi N)_{ODT} \geq 10.5$ and that the interlamellar domain spacing scales as $d \sim \chi^{1/6} N^{2/3}$.

In contrast, block copolymers containing crystallizable components may undergo microphase separation due to (i) chemical incompatibility between the two blocks resulting in a *heterogeneous* melt or (ii) crystallization of one block and attendant expulsion of the other block from the crystalline structure, i.e., a *crystallization-induced* microphase separation from a *homogeneous* melt. When the block copolymer is microphase-separated in melt, the final morphology of the semicrystalline state depends on the block copolymer segregation strength, χN. If the ordered structure is strongly segregated in the melt, crystals grow within the confines of the structure prescribed by f and χN prior to crystallization.[8] If the ordered structure is weakly segregated, crystallization breaks out of the equilibrium morphology formed in the heterogeneous melt, and it induces a new lamellar structure independent of block copolymer composition as reported by the groups of Nojima,[9] Ryan,[10] and Hamley.[11] In the case of homogeneous block copolymer melts, crystallization precedes formation of ordered structures arising from chemical incompatibility. Therefore, a microphase-separated state develops during the process of crystallization. In a manner similar to weakly segregated heterogeneous melts, these homogeneous melts crystallize to form lamellar morphologies over a wide range of compositions in the solid state.[12]

Two theories concerning the equilibrium morphology of symmetric crystalline−amorphous diblock copolymers in the solid state were developed to predict the molecular weight dependence of the characteristic interdomain thickness. By assuming a lamellar morphology in the strong segregation limit with equal densities and statistical segment lengths for both blocks, DiMarzio, Guttman, and Hoffman (DGH)[13] derived a decoupled scaling law for the equilibrium combined thickness of the crystalline and the amorphous domains:

$$d \sim N_t N_a^{\beta}$$

where N_t is total molecular weight of the diblock, N_a is the molecular weight of amorphous block, and the scaling exponent $\beta = -1/3$. Using mean-field theory, Whitmore and Noolandi (WN)[14] derived a similar scaling law with $\beta = -5/12$.

Reports addressing the experimental validity of the theoretically predicted DGH and WN scaling laws appeared in the early 1990s,[12,15−17] before the melt phase behavior of diblock copolymers became well-established. Douzinas et al.[15] reported that microphase-separated poly(ethylene-*co*-1-butene)−poly(ethylethylene) diblock copolymers with various compositions satisfied the aforementioned decoupled scaling form with $\beta = -(0.42 \pm 0.02)$. Nojima et al.[16] obtained a

[†] Department of Chemical Engineering and Materials Science.
[‡] Department of Chemistry.
* Corresponding author: e-mail bates@cems.umn.edu.

10.1021/ma0501794 CCC: $30.25
Published on Web 06/11/2005

Table 1. BIB Molecular Characterization Data

	^{1}H NMR				GPC	
polymer	f_{PB}	1,2 PB (%)	ethyl branches/1000 carbon	4,3 PI (%)	M_w (kg/mol)	M_w/M_n
PB	1.00	8.0	21		118	1.05
BIB27K	0.47	8.4	22	5.8	27	1.03
BIB35K	0.47	8.4	22	5.8	35	1.07
BIB46K	0.47	7.6	20	4.7	46	1.05
BIB73K	0.48	8.0	21	5.0	73	1.04
BIB103K	0.49	6.6	17	3.9	103	1.02
BIB145K	0.49	7.0	18	4.4	145	1.06
BIB251K	0.48	8.7	23	6.0	251	1.06
BIB372K	0.47	6.9	18	7.0	372	1.25

scaling exponent of $\beta = -0.54$ for the poly(ϵ-caprolactone)−poly(butadiene), and Unger et al.[17] observed a scaling exponent of $\beta = -(0.53 \pm 0.19)$ in poly(ethylene oxide)−poly(*tert*-butyl methacrylate) which may vary substantially from theory due to unequal statistical segment lengths. Rangarajan et al.[12] obtained a scaling exponent of $\beta = -(0.45 \pm 0.07)$ by using EP diblock copolymers in which crystallization-induced microphase separation occurs, a result that numerically agrees with the WN prediction. However, the authors of the last report concluded that their results were inconsistent with the theoretical predictions due to inconsistencies between the experimentally observed crystal morphologies and those assumed within the DGH and WN models. Since all of these studies utilized diblock copolymers with a variety of compositions, the effect of the segregation strength of the melt from which crystallization occurred was not systematically considered.

Some experimental work[18,19] has revealed the dependence of the final microstructure upon crystallization in semicrystalline block copolymers on the segregation strength of the melt or solution from which they are crystallized. For a poly(styrene)−poly(ethylene-*co*-1-butene) diblock copolymer containing 11 wt % of the crystallizable E-block solvent cast from toluene, Cohen et al.[18] reported that the final morphology depends on sample history, more explicitly, the casting temperature and annealing temperature. Additionally, Seguela and Prud'homme[19] also reported that the chain folding direction of the E crystallites in the E domains of an EPE triblock copolymer (27 wt % E) was affected by the processing history, which may account for the weaker tensile properties of the solution-crystallized samples relative to those crystallized from the melt.

The effects of block copolymer composition and molecular weight and resulting morphology on the ultimate mechanical properties of thermoplastic elastomers have been extensively studied.[20−27] In the case of amorphous ABA triblock copolymers composed of glassy end blocks and a rubbery center block, the strength of the materials correlates strongly with the that of the glassy end blocks since brittle fracture of these domains is postulated to be the dominant fracture mechanism.[23,25] Lim et al. recently extended this result to the case of CEC and CECEC block copolymers (C = poly(cyclohexylethylene)), in which a semicrystalline linear low-density polyethylene domain bridges the glassy domains.[27] The mechanical properties of crystalline−rubbery−crystalline type block copolymers have not been systematically explored in depth. Reports by the groups of Falk,[28,29] Seguela,[19] and Mohajer[30] disclosed the mechanical properties of crystalline−rubbery−crystalline type thermoplastic elastomers without careful attention to the effects of microstructure and morphology. Lovinger et al. examined the crystallization behavior and solid-state structure of poly(ϵ-caprolactone)−poly(dimethylsiloxane)−poly(ϵ-caprolactone); however, mechanical properties of these materials were not disclosed.[31]

In this study, a series of symmetric EPE triblock copolymers with molecular weights ranging from 27 to 372 kg/mol have been investigated in order to explore the influence of melt segregation strength on the observed equilibrium morphologies and solid-state microstructures of these materials along with their attendant mechanical properties. We restrict our study to symmetric compositions, $f_E \approx f_P \approx 0.5$, so that polymer composition effects are excluded.

Experimental Section

Synthesis and Molecular Characterization. Synthesis of Symmetric EPE Triblock Copolymers. Symmetric poly(1,4-butadiene)−poly(1,4-isoprene)−poly(1,4-butadiene) (BIB) triblock copolymers were synthesized by sequential anionic polymerization in purified cyclohexane at 40 °C initiated by *sec*-butyllithium. Detailed procedures for anionic polymerizations may be found elsewhere.[32]

Quantitative ^{1}H NMR spectra of the polymers dissolved in $CDCl_3$ were recorded on a Varian Unity Inova 300 spectrometer with a pulse repetition delay of 10 s to determine the weight fraction of the butadiene block (f_{PB}), the percent 1,2-addition in the polybutadiene block, and the percent 3,4-addition in the polyisoprene block listed in Table 1. All BIB triblocks have almost constant weight fractions of butadiene (0.5) and 6.6−8.7 mol % of 1,2-units in the polybutadiene blocks, corresponding to 17−23 ethyl branches per 1000 backbone carbons in the B block, and 5−8 mol % of 3,4-units in the polyisoprene block.

The molecular weight of each sample determined by room temperature GPC-LS using THF as the eluent agrees (within ±3%) with the value calculated from the molecular weight of the first B block and the monomer feed for each block. (Because of the similarity of the refractive index increments dn/dc for polybutadiene and polyisoprene in THF (0.130 and 0.124 cm^3/g, respectively), the light scattering data were analyzed using a single value dn/dc = 0.127 cm^3/g to determine M_w and M_w/M_n for each sample.) The molecular weight distributions of all of the BIB triblock copolymers are narrow, with $M_w/M_n \leq 1.07$ except that of BIB372K, for which $M_w/M_n \leq 1.25$ (see Table 1).

Catalytic hydrogenation of the BIB polymers at 140 °C in degassed cyclohexane under 500 psig H_2 for 12 h using a Pt/Re catalyst supported on wide-bore silica (Dow Chemical Co.) provided the desired symmetric EPE triblocks in quantitative yields.[33] After catalytic heterogeneous saturation, the EPE triblock copolymers exhibit unimodal molecular weight distributions and narrow polydispersities as determined by high-temperature SEC at 140 °C in 1,2,4-trichlorobenzene, thus demonstrating that the hydrogenation process does not lead to chain degradation. The degree of hydrogenation of EPEs as determined by FT-IR analysis was >99%.

Morphological Characterization. Thermal Analysis. Differential scanning calorimetry was performed on polymer samples using a Thermal Analysis Q1000. The thermal history of the samples was erased by heating to 140 °C for 5 min before

Table 2. EPE Morphological Characterization Data

	DSC			WAXS			SAXS			
polymer	T_m	T_g	ω_c	a (Å)	b (Å)	ω_c	interdomain spacing, d(nm)	crystal lamella thickness, d' (nm)	crystal thickness, l_c (nm)	predicted crystal thickness, l_c (nm)
PE	104.4		0.33	7.59	5.04	0.40		14.0	5.6	5.6
EPE27K	103.4	−61.0	0.40	7.51	4.99	0.42	27.0			5.6
EPE35K	104.4	−60.9	0.39	7.46	4.95	0.43	28.8			5.8
EPE46K	104.4	−62.0	0.42	7.52	4.98	0.41	30.1			5.8
EPE73K	104.5	−61.7	0.33	7.53	5.01	0.37	34.1			6.0
EPE103K	104.3	−60.4	0.40	7.54	5.01	0.37	36.1			6.5
EPE145K	103.5	−60.9	0.36	7.52	4.97	0.38	45.1	15.4	7.5	8.4
EPE251K	103.8	−63.9	0.33	7.52	4.96	0.37	64.8	15.0	7.4	11.5
EPE372K	100.9	−61.0	0.34	7.53	4.99	0.37	80.2	15.0	7.1	14.0

cooling to −100 °C at 10 °C/min. Second heating and cooling data were then collected at 10 °C/min.

WAXS. Wide-angle X-ray scattering (WAXS) was performed using the Bruker AXS (Siemens) microdiffractometer for 2D WAXS and a Siemens D5005 for 1D WAXS. 2D WAXS studies employed a sample-to-detector distance of 6.0 cm.

SAXS. Synchrotron small-angle X-ray scattering measurements were performed at the 5ID-D beamline of the DuPont-Northwestern-Dow (DND-CAT) Synchrotron Research Center located at the Advanced Photon Source, Argonne National Laboratory. A beam energy of 8 keV (λ = 1.54 Å) and a sample−detector distance of 3.026 m were used. The EPE samples were prepared by heating to 140 °C and cooling at the rate of 0.1 °C/min to room temperature under nitrogen.

Laboratory source SAXS measurements were performed at the Institute of Technology Characterization Facility at the University of Minnesota, using copper Kα X-rays generated by a Rigaku RI-200VBH rotating anode with a sample-to-detector distance of 3.50 m.

Dynamic Mechanical Spectroscopy. Order−disorder phase transition temperatures (T_{ODT}) were determined by dynamic mechanical spectroscopy (DMS) measurements performed using a Rheometrics Scientific ARES strain-controlled rheometer fitted with 8 mm diameter parallel plates. Heating rates of 1 °C/min were used for isochronal temperature ramp tests to determine T_{ODT}.

Shear Alignment. A "single-grain" sample of triblock copolymer EPE251K was produced by shear alignment using a reciprocating shear device similar to that described by Koppi et al.[34] The sample was heated to (T_{ODT} − 10) ° C under nitrogen and subjected to a shear rate of 0.05 s^{-1} with γ = 10 for 1 h, followed by slow cooling to room temperature under nitrogen.

Transmission Electron Microscopy. TEM was performed using a JEOL 1210 transmission electron microscope operating at 120 keV in the bright field mode. Samples were stained according to established procedures.[35] Briefly, samples were cryo-microtomed at −120 °C before staining to create a flat surface face and immersed into ruthenium tetraoxide (RuO_4) solution for at least 10 h to obtain sufficient staining contrast. Stained thin films (50−90 nm) were then obtained by cryo-microtoming at −120 °C for TEM analysis.

Mechanical Testing. Tensile deformation experiments (engineering stress $\sigma = F/A_0$ vs strain ϵ (%) = $(l - l_0)/l_0$) were carried out at room temperature using a Rheometrics Scientific Minimat instrument operating at a crosshead speed of 5 mm/min. Because of limited sample availability, nonstandard sample dimensions were used: 5 mm gauge length, 3.0 mm gauge width, and 0.30 mm thickness. Type V ASTM tensile bars described in the ASTM standard D638 were also tested and behaved similarly to the nonstandard tensile samples employed in this study.

Results

Thermal characterization data for the EPE triblock copolymers synthesized in this study are listed in Table 2. The peak melting temperature $T_{m,E}$ of the polyethylene blocks in the EPE samples is comparable to that of the linear low-density polyethylene produced hydrogenation of 1,4-polybutadiene homopolymer. The glass transition temperature of the hydrogenated 1,4-polyisoprene blocks, $T_{g,P}$ = −61 °C, also compares favorably with the literature value expected for this polymer. These data indicate that the E and P domains are microphase-separated at low temperature in all EPE samples. The weight fraction crystallinity, ω_c, of the E blocks was calculated from heat of fusion, ΔH_m, using the following equation:

$$\omega_c = \Delta H_m / \Delta H_{m,E} f_E \quad (1)$$

where f_E is the weight fraction of polyethylene, and $\Delta H_{m,E}$ = 277 J/g is the theoretical heat of fusion of 100% crystalline high-density polyethylene.[36]

Wide-angle X-ray scattering (WAXS) permits the measurement of the unit cell dimensions of E crystallites in E homopolymer as well as EPE triblock copolymers (see Figure 1). The sharp diffraction peaks observed by WAXS correspond to the (110) and (200) reflections from the orthorhombic unit cell of polyethylene, while the broad peak results from amorphous E and P domains. On the basis of the unit cell dimensions derived from the WAXS data, the size of polyethylene crystals present in the EPE triblocks is the same as those observed in E homopolymer within experimental error.

WAXS data corroborate the crystalline weight fractions of the E domains in these polymers obtained from DSC analysis. The crystallinity of EPE was calculated using the equation

$$\omega_c = (I(110) + I(200))/I_{total} f_E \quad (3)$$

where I(110) and I(200) correspond to the intensities of the (110) and (200) reflections, I_{total} is the total observed

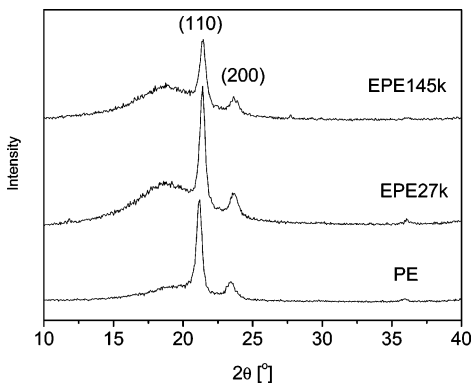

Figure 1. WAXS patterns of homopolyethylene, EPE27K, and EPE145K.

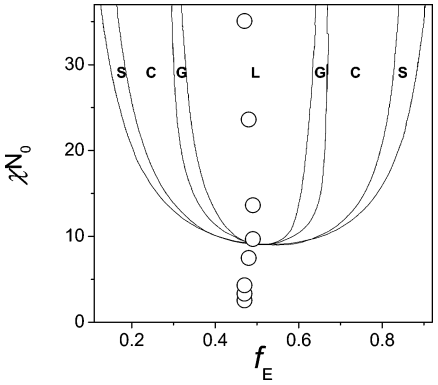

Figure 2. χN_0 of EPEs are plotted by open circle symbols (○) on a reproduction of Matsen and Thomson's phase diagram[5] at 85 °C. The ordered phases are labeled as L (lamellar), G (gyroid), C (cylinder), and S (spherical).

Table 3. χN_0 and T_{ODT} of EPE by Theoretical Calculation and Experiments

polymer	$N_0 \times 10^{-3}$	χN_0 at 85 °C	calcd T_{ODT} (°C)	measd T_{ODT} (°C) by ARES
EPE27K	0.26	2.6	−80	$<T_m$
EPE35K	0.34	3.3	−46	$<T_m$
EPE46K	0.44	4.3	−12	$<T_m$
EPE73K	0.76	7.5	61	$<T_m$
EPE103K	0.99	9.7	96	$<T_m$
EPE145K	1.39	13.6	131	114
EPE251K	2.41	23.6	180	169
EPE372K	3.58	35.1	206	

intensity, and f_E is the weight fraction of E in the sample. The crystallinities of EPEs measured by WAXS and DSC are consistent and comparable to that of homopolyethylene ($\omega_c \approx 0.4$) with no significant dependence on M_n.

The order−disorder transition temperature T_{ODT} of each EPE triblock was determined by two rheological methods: the time−temperature superposition of isothermal frequency sweeps performed at different temperatures and isochronal temperature ramp tests. The order−disorder transition is associated with a sudden drop in the elastic modulus, G', in isochronal temperature ramp tests and a distinct change from terminal ($G' \sim \omega^2$) to nonterminal behavior ($G' \sim \omega^{0.5}$) in isothermal frequency sweep data above and below T_{ODT}.[37,38] The order−disorder transition temperatures for EPEs with $M_n \geq 145$ kg/mol measured by these methods are listed in Table 3. The T_{ODT} for EPE372K was not determined due to problems associated with thermal degradation. For EPE triblocks with $M_n < 145$ kg/mol, T_{ODT} could not be measured due to the onset of crystallization in the E domains before microphase separation occurs, that is, $T_{c,E} > T_{ODT}$, where $T_{c,E}$ is the crystallization temperature of the E domains.

To evaluate the microphase separation mode of each EPE triblock copolymer, χN_0 for each EPE was plotted on a reproduction of the theoretically predicted triblock copolymer phase diagram of Matsen and Thompson[5] (see Figure 2 and Table 3). A reference temperature of 85 °C in Figure 2 was chosen since $T_{c,E} \sim 85$ °C for the EPE triblocks in this study. To account for the triblock architecture, we calculated $N_0 = M_n/(2m_0)$, where M_n is the total number-average molecular weight of EPE triblock copolymer, $m_0 = 56$ Da is the molecular weight of the monomer normalized to the 118 Å^3 monomer reference volume, and the factor of 2 accounts for the

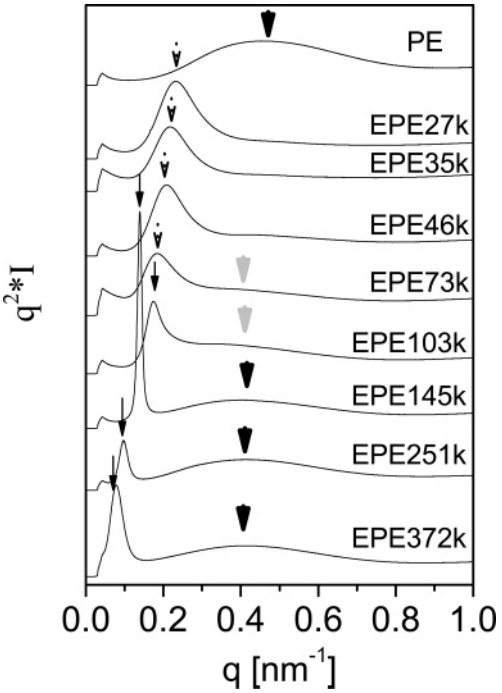

Figure 3. Synchrotron SAXS patterns of homo-PE and EPEs at room temperature.

triblock architecture. χ was calculated on the basis of Koppi's result:[34]

$$\chi = 10.3/T - 0.019 \quad (4)$$

Using the mean-field theory result $(\chi N_0)_{ODT} = 9.0$, derived by Mayes and Olvera de la Cruz[6] for symmetric triblock copolymers with equal statistical segment lengths, T_{ODT} for each EPE can be quantitatively estimated as listed in Table 3. The calculated values of T_{ODT} are consistent with the experimental results, affirming the applicability of this equation to EPE triblock copolymers. In the phase diagram presented in Figure 2, high molecular weight samples EPE145K, EPE251K, and EPE372K lie in the melt microphase-separated region, implying that the samples crystallize from the heterogeneous, microphase-separated state. In contrast, the low molecular weight samples EPE27K, EPE35K, and EPE46K are not microphase separated in the melt; hence, crystallization of the E blocks occurs from a homogeneous melt because the crystallization precedes the microphase separation. EPE73K and EPE103K are close to the microphase separation transition line in the phase diagram.

Figure 3 shows synchrotron SAXS patterns of homo-E and EPEs taken at room temperature. Because of the nearly identical electron densities of E and P domains in the melt, the microphase-separated EPE triblocks initially display only a small amount of X-ray contrast in the melt. Crystallization of E block, however, creates a substantial electron density difference between the domains, thus leading to the increased SAXS intensity. Two reflection peaks are observed for EPE145K, EPE251K, and EPE372K, which microphase-separate prior to crystallization: (i) a broad and weak peak at the high values of q independent of molecular weight and (ii) an intense and sharp peak at a low value of q dependent upon the overall molecular weight. The broad peak centered at $q = 0.42$ nm^{-1} ($d = 15.0$ nm) stems from the inter-E-crystal lamellar thickness (d') in the

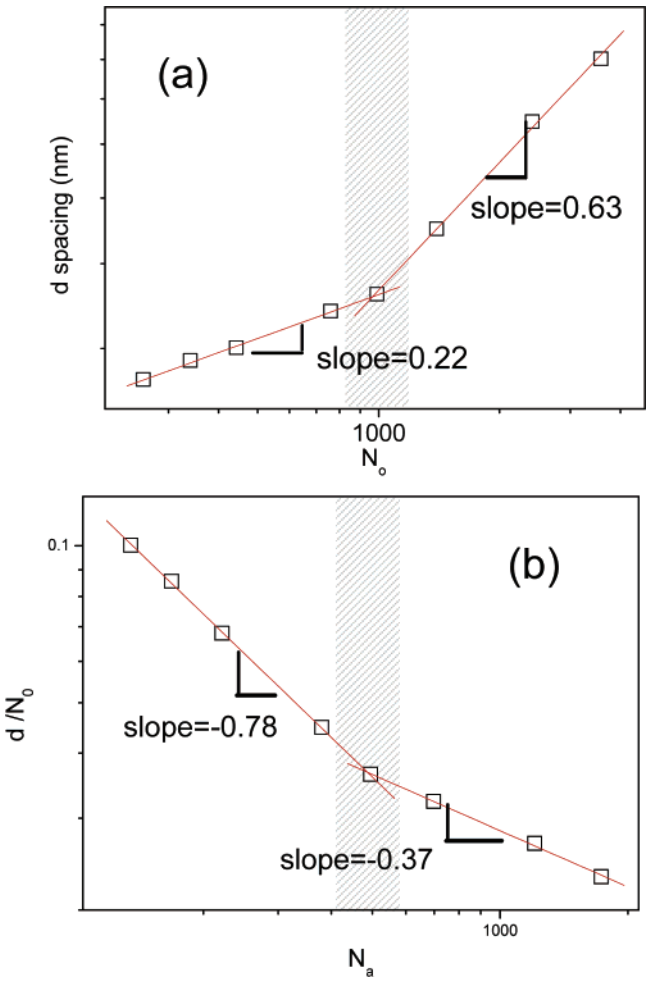

Figure 4. (a) Domain spacing (d) vs molecular weight (N_0) plot for comparison with the scaling law for amorphous−amorphous block copolymer and (b) d/N_0 vs N_a plot for comparison with WN and DGH scaling laws for crystalline−amorphous block copolymer.

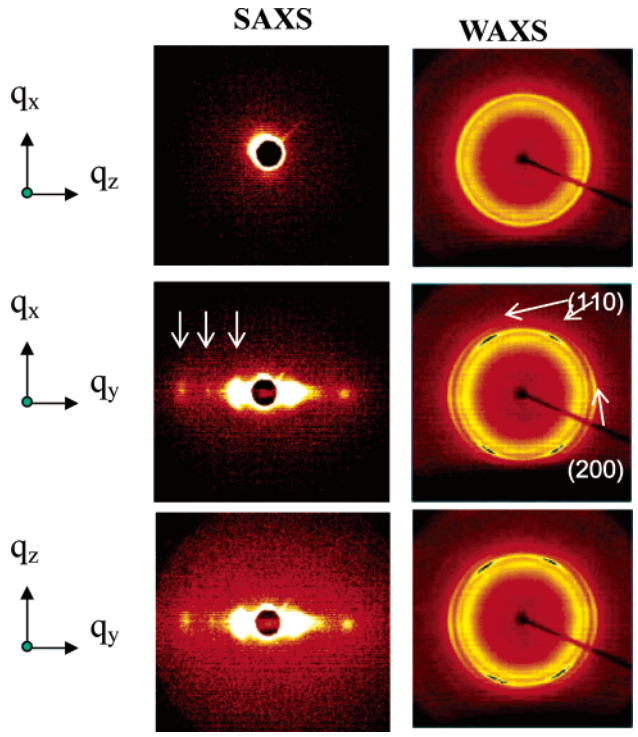

Figure 5. WAXS and SAXS patterns of shear-aligned EPE251K at room temperature. The sample was prepared using a reciprocating shear device with strain amplitude of $\gamma = 10$ and shear rate of 0.05 s^{-1} at $T_{ODT} - 10$ °C for 1 h under nitrogen, and then sample was slowly cooled to the room temperature. x-axis is shear direction, and y-axis is velocity gradient direction.

E domain. This scattering peak assignment is confirmed by the observation that E homopolymer exhibits a single broad peak with peak maximum at $q = 0.45$ nm^{-1} ($d = 2\pi/q = 14.0$ nm), where the breadth of the peak indicates the presence of a distribution of crystallite dimensions. The E-crystal lamellae in the EPE triblock copolymers are only slightly larger than those of homopolyethylene. The intense peak at low q originates from the overall lamellar domain spacing d, which depends on the total M_n for the triblock copolymer (vide infra). Higher order scattering peaks from this supramolecular lamellar structure are not observed. In contrast, EPE27K, EPE35K, and EPE46K, which exhibit crystallization-induced microphase separation, display one peak at an intermediate q value which may result from the convolution of two peaks (d and d'). This peak is much broader than the first intense peak of EPE145K, EPE251K, and EPE372K. EPE73K and EPE103K show the intermediate patterns having an intense peak and a weak and broad hump at the intermediate q values.

Domain spacings, d, obtained from the room temperature SAXS data presented in Figure 3 are plotted vs N_0 in Figure 4a, in which the gray region indicates the microphase separation transition region. Two distinct scaling regimes are readily identified in this plot. At high molecular weights, where chemical incompatibility-induced microphase separation occurs, the domain spacing scales as $d \sim N_0^{0.63}$. This behavior agrees well with the mean-field theory prediction that $d \sim N^{2/3}$ for strongly segregated amorphous−amorphous block copolymers.[1−4] At the low molecular weights, for which crystallization-induced segregation dominates microdomain structure formation, the domain spacing scales as $d \sim N_0^{0.22}$. The observed scaling exponent 0.22 is surprisingly small, in view of the fact that the end-to-end distance for a Gaussian polymer coil is proportional to $N_0^{1/2}$.

For comparison with the DGH[13] and WN[14] scaling laws for the interlamellar domain spacings of crystalline−amorphous diblock copolymers, the experimental data are replotted in Figure 4b as d/N_0 vs N_a. Again, two different scaling behaviors are evident: $d \sim N_0 N_a^{-0.37}$ in the chemical incompatibility-induced microphase separation regime and $d \sim N_0 N_a^{-0.78}$ in the crystallization-induced microphase separation regime. The incompatibility-induced scaling exponent −0.37 lies between theoretically predicted values of −0.33 (DGH) and −0.42 (WN), while the crystallization-induced scaling exponent −0.78 disagrees with the theoretical value. This last result is also different from the scaling exponent $\beta = -(0.45 \pm 0.07)$ obtained by Rangarajan et al. for EP diblock copolymers which also undergo crystallization-induced phase separation.

To more thoroughly investigate the chain-folded structure of the polyethylene crystals within the microdomains formed upon crystallization of a melt microphase-separated block copolymer, a "single grain" EPE sample was prepared by shear alignment. Figure 5 shows SAXS and WAXS patterns of shear-aligned EPE251K at the room temperature. The SAXS patterns display well-defined reflections along the scattering

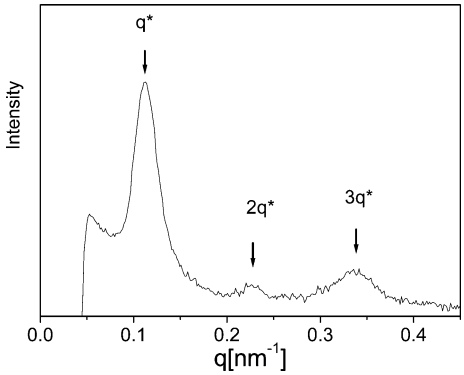

Figure 6. SAXS pattern of shear-aligned EPE251K from *yz*-plane.

vector q_y indicative of long-range order. In the one-dimensional plot of $I(q)$ vs q obtained from the radial integration along the q_y direction in the q_z-q_y plane shown in Figure 6, the observed Bragg scattering peaks corresponding to q^*, $2q^*$, and $3q^*$ are consistent with a well-aligned lamellar morphology. The value of q^* for the shear-aligned EPE is slightly larger than that of isotropic sample shown in Figure 3. The lamellae normal is directed along the velocity gradient direction (y), indicating that EPE251K has a "parallel" orientation. The TEM micrograph of shear-aligned EPE251K microtomed parallel to the x-direction presented in Figure 7a confirms the parallel-oriented lamellar morphology deduced from the SAXS data. The bright regions correspond to crystalline E domains (crystallinity inhibits uptake of RuO_4), while the dark stained regions are the rubbery P domains. The sharp lamellar interfaces seen in Figure 7a demonstrate that E crystallization is confined within and does not disrupt the lamellar structure. The 2D WAXS patterns of the shear-aligned EPE251K shown in Figure 5 exhibit three reflections: sharp peaks associated with the (110) and (200) planes of the orthorhombic unit cell in E crystals and one broad peak assigned to the amorphous P and amorphous E domains; this analysis is analogous to that presented for the data in Figure 1. The (110) peaks are oriented at an azimuthal angle $\phi = 56°$ relative to the horizontal direction (q_y), and the (200) peaks are aligned with the velocity gradient direction (q_y) in the q_x-q_y and q_z-q_y planes. Additionally, (200) does not appear in the q_x-q_z plane. These results imply that the E-crystal stems lying along the c-axis of the unit cells are aligned parallel to the lamellae, consistent with previous results of Cohen et al.[39,40]

Figure 7b shows a representative TEM image of the crystallization-induced microphase-separated morphology in an EPE triblock copolymer. EPE27K has an alternating lamellar morphology with regular domain spacing, $d \sim 30$ nm, in favorable agreement with the SAXS result (see Table 2). Sheaflike structures comprised of spherulites (not shown) are observed in the TEM images. The domain structure in this material resembles that found in linear low-density poly(ethylene), for which the final morphology is dominated by nucleation and growth mechanisms of crystallization.

Figure 8a shows the strain−stress curves of E homopolymer and EPE triblock copolymers. Homopolyethylene produced from hydrogenated poly(butadiene) has a tensile modulus ($E = 41$ MPa), a tensile strength ($\sigma_B = 35.5$ MPa), and an elongation at break ($\epsilon_B \sim 800\%$) which are close to those of low-density polyethylene.[36]

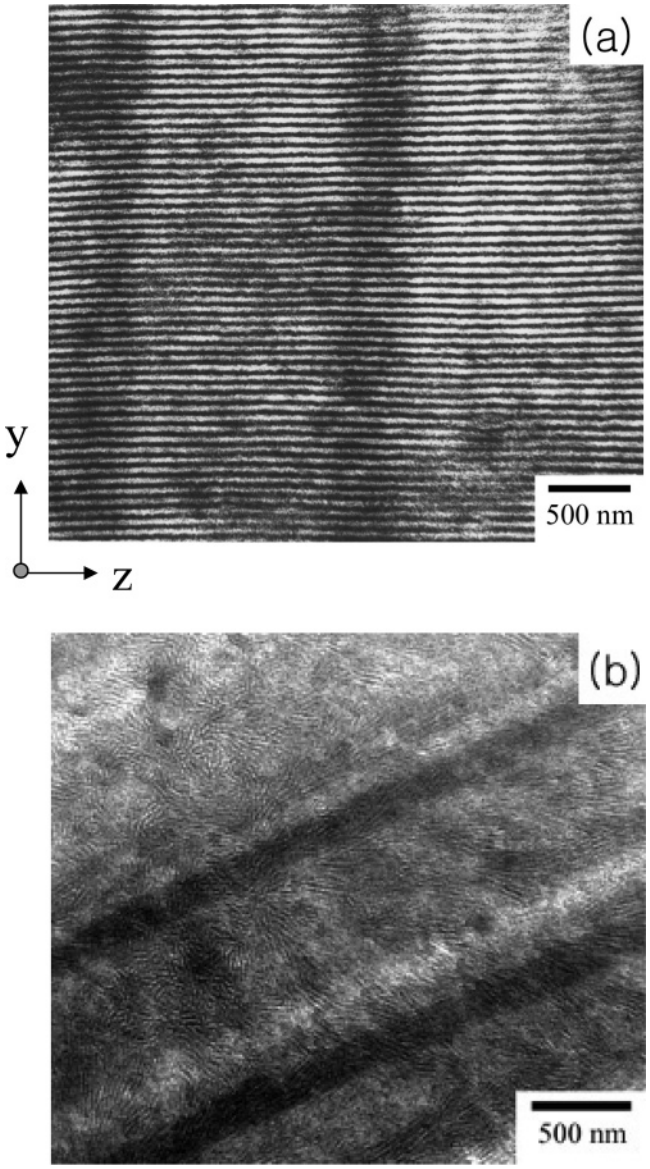

Figure 7. Transmission electron micrograph of (a) shear-aligned EPE251K with *yz*-plane and (b) EPE27K.

EPEs follow the similar stress−strain curves that of the E homopolymer. None of the EPEs show necking behavior, and all of them exhibit almost constant tensile moduli, $E \sim 14$ MPa, regardless of molecular weight. The ultimate tensile properties of EPE triblock copolymers presented in Figure 8 significantly depend on the total molecular weight and can be classified into three regimes of behavior. Low molecular weight samples EPE27K, -35K, and -46K are very brittle and weak (EPE27K and -35K are not shown here) with $\epsilon_B < 30\%$ strain and $\sigma_B < 2.1$ MPa and break even before the onset of plastic deformation. At the opposite end of the spectrum, high molecular weight samples EPE145K, -251K, and -372K show a high ductility and strength ($\epsilon_B > 800\%$ strain and $\sigma_B > 20$ MPa). In this regime, ϵ_B and σ_B appear almost independent of molecular weight. For EPE73K and -103K samples with intermediate molecular weight, ϵ_B and σ_B steeply increase with the molecular weight.

Discussion

The mode of microphase separation and the consequent solid-state microdomain structure for semicrys-

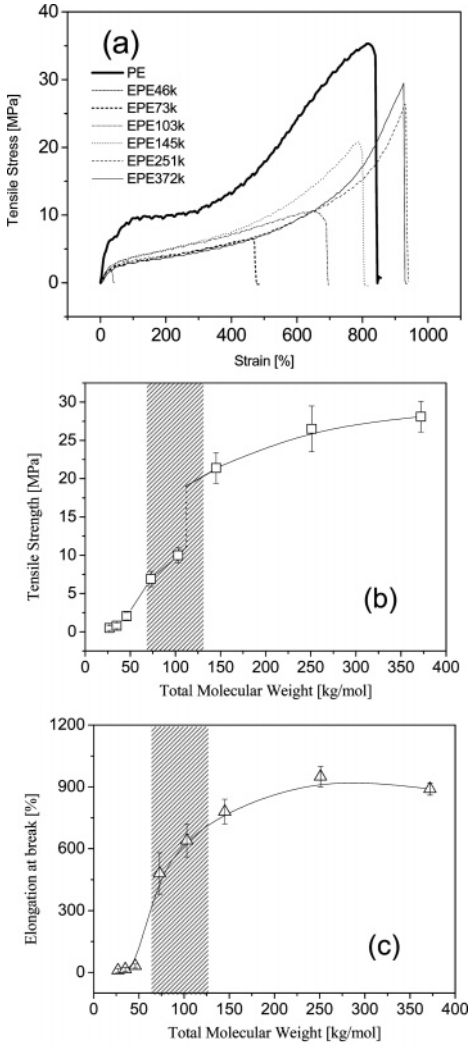

Figure 8. (a) Stress−strain curves of homopolyethylene and EPEs and (b) ultimate tensile strength and (c) elongation of EPEs as a function of molecular weight.

talline EPE triblock copolymers depend sensitively on the total molecular weight of the block copolymer. High molecular weight EPEs are microphase separated due to the chemical incompatibility between E and P blocks in the melt from which crystallization occurs ($T_{ODT} > T_{c,E}$). On the other hand, low molecular weight EPEs crystallize from a homogeneous melt because microphase separation does not occur before the onset of crystallization of the semicrystalline E blocks ($T_{c,E} > T_{ODT}$). In the latter case, the strong driving force for crystallization in the E blocks causes the P segments to be excluded from the crystallites inducing microphase separation. The different microphase separation modes produce different experimentally observed scaling laws for the predicted lamellar domain spacing for compositionally symmetric block copolymers: $d \sim N_0^{0.63}$ ($d \sim N_0 N_a^{-0.37}$) for incompatibility-induced microphase separation, and $d \sim N_0^{0.22}$ ($d \sim N_0 N_a^{-0.78}$) for crystallization-induced microphase separation. Elucidation of the relationship between the mode of microphase separation and the microdomain structures yields insights into the differences that give rise to the different power laws governing lamellar domain spacings.

The final microstructure of the semicrystalline E domains of strongly segregated EPE triblock copolymers can be definitively assigned on the basis of the combination of SAXS, WAXS, and TEM data presented in this

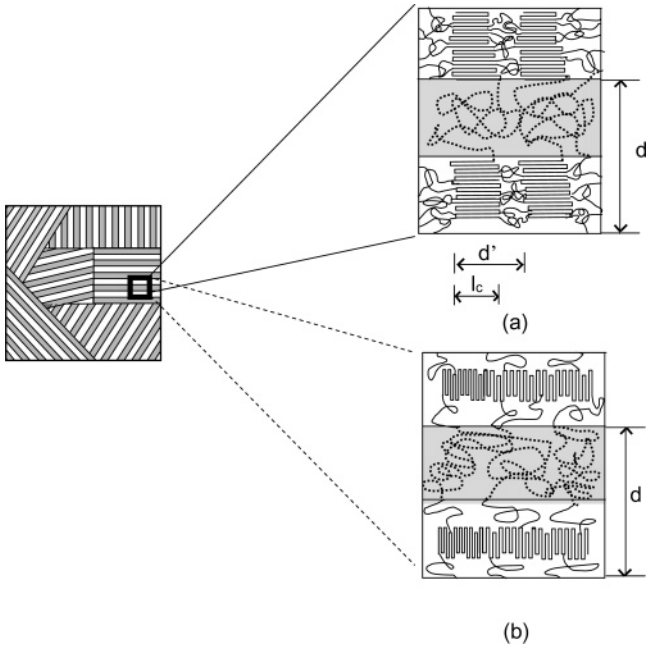

Figure 9. Illustration of proposed microstructures for EPE triblock copolymers. (a) EPE crystallized from a heterogeneous melt. d is the total lamellar domain spacing, d' is the E-crystal lamellar thickness, and l_c is E-crystal thickness. (b) EPE crystallized from a homogeneous melt.

study. Symmetric EPEs with incompatibility-induced microphase separation display a lamellar morphology in which E and P domains are well segregated in the melt with a characteristic domain spacing d. As a result of the high segregation strength of this heterogeneous melt, crystallization in the E domains is strongly confined and does not disrupt the lamellar morphology. WAXS studies of a shear-aligned "single-grain" EPE251K sample show that the polymer chains in the E-crystals are oriented parallel to the planes of interdomain lamellar structure so that E-crystal lamellae with an average fold thickness d' are oriented perpendicular to the interdomain lamellae. On the basis of these observations, we formulate the microdomain structural model depicted in Figure 9a, for which there are three relevant length scales: the E-crystal thickness l_c, the intercrystal lamellar thickness d', and interdomain lamellar spacing d. Notably, the direction of chain folding is quite different from that observed when crystallization occurs by a nucleation and growth mechanism from a homogeneous polymer melt; in the latter crystallization mode, the polymer chains orient perpendicular to the planes of lamellar structure.

In predicting the scaling laws for crystalline−amorphous diblock copolymer interdomain lamellar thickness, the DGH and WN models assume that the crystallizable chains are oriented perpendicular to the plane of interdomain lamellar structure. Despite the difference in the experimentally observed morphology and that assumed by theory, the observed scaling relation $d \sim N_0 N_a^{-0.37}$ is in a good agreement with the prediction. In addition, the scaling relation $d \sim N_0^{0.63}$ agrees well with the mean-field theory of Helfand for strongly segregated completely amorphous block copolymers.[2,3] These correlations suggest that the strong melt-phase segregation before crystallization contributes more strongly to the ultimate domain spacing in the solid state than the chain-folded structure.

On the basis of conventional nucleation and growth mechanisms for crystallization of homopolymer melts, we expect symmetric EPEs that undergo crystallization-induced microphase separation from a homogeneous melt to exhibit a lamellar morphology in which polymer chains in E-crystals are oriented perpendicular to the plane of interdomain lamellar structure. Consequently, E-crystal lamellae with an average fold thickness d' are oriented parallel to the interdomain lamellae, as illustrated in Figure 9b. Under the constraints of this model, the E-crystal thickness l_c listed in last column of Table 2 can be calculated from

$$l_c = \omega_c f_E d \tag{5}$$

where the crystallinity ω_c is derived from WAXS results (Table 2). The values of l_c for EPE27K, EPE35K, EPE46K, and EPE73K are close to that of homopolyethylene ($l_c \sim 5.6$ nm). Since the size and ordering of crystallites are exclusively determined by the number of ethyl branches on the backbone chain and all of the EPE samples have the approximately equal numbers of ethyl branches per 1000 backbone carbons (20 ± 3 in the E blocks), they are expected to have the same crystal thickness l_c as E homopolymer. This supports the notion that crystallization-induced microphase separation exhibits the conventional chain folding structure as drawn in Figure 9b. The observation of a single length scale associated with the SAXS patterns for EPE27K, EPE35K, and EPE46K is also consonant with the proposed chain-folding model. As M_n decreases, the E domain thickness (calculated to be $f_E d$) approaches a limiting value equal to the crystal lamellar thickness $d' = 14$ nm observed for E homopolymer, thus disallowing the stacking of E crystals into multiple layers within the E domain. The absence of scattering peaks indicative of intercrystal amorphous regions at high values of q suggests that the crystals are closely stacked together so that the chain axes are perpendicular to the lamellar structure induced by crystallization. This implies either that the amorphous E regions are at the interface with the amorphous P regions or that the amorphous E and P are mixed. Therefore, only one reflection from the interdomain lamellar spacing d between the amorphous and crystalline domains of the segregated morphology is observed. This peak is much broader than that observed in the case of incompatibility-induced microphase separation since the operative mode of crystallization-induced microphase separation depends on the kinetics of crystallization. (The possibility of fortuitous overlap of peaks associated with the intercrystal distance and the interlamellar domain structure induced by crystallization is discounted on the basis of the trends in the SAXS data in Figure 3, which demonstrate that as M_n decreases, the low q scattering maximum broadens and shifts to moderate q and the broad peak associated with polyethylene crystallinity decreases in intensity and vanishes.)

The disagreement between the DGH and WN predictions and the experimentally observed domain spacing dependence upon molecular weight in the crystallization-induced segregation regime for EPE triblock copolymers likely originates in the theoretical assumptions surrounding the crystallization events. Both theories assume that final chain-folded state of the crystallized block copolymer melt is an equilibrium state dictated by the interfacial energy balance between the crystallizable and amorphous blocks, in which each crystalline chain fold spans the entire crystalline domain. Since the ethyl branch content of the linear low-density PE block controls the chain folded morphology, with little or no contribution from kinetic phenomena, the crystal stems of intermediate molecular weight polymers are not long enough to span the crystalline domains, and on average more than one crystal thickness is accommodated. Thus, a fundamental assumption of the theoretical models is violated, and it is not surprising that the scaling law $d \sim N_0^{0.22}$ ($d \sim N_0 N_a^{-0.78}$) disagrees with known theories. In the low molecular weight limit, one expects the E-crystallite size to be invariant with respect to molecular weight so that the thickness of the E domain would remain constant. Assuming that the interfacial area between the E and P domains remains constant, the thickness of the P domain must remain constant since $f_E \approx f_P \approx 0.5$. Hence, the domain scaling law should be $d \sim N_0^0$, as observed for EPE27K and EPE35K.

Rangarajan et al.[12] have previously observed that the domain spacing obtained from crystallization-induced segregation of EP diblock copolymers from homogeneous melts over a variety of compositions obeys the scaling law $d \sim N_0 N_a^{-(0.45\pm0.07)}$, in disagreement with theory due to violation of the theoretical assumptions (see above). The larger disagreement between our result and preexisting theoretical and experimental work may stem from the triblock molecular architecture employed in this study. While previous theories make quantitative predictions for diblock copolymers, the analogous problem for triblock copolymers has not been considered. The latter situation is unique in that both ends of the amorphous domain are pinned at interfaces with the crystalline domains. Consequently, the extent to which PE crystal stems span complete crystalline domains may differ on the basis of the constraints enforced by the polymer chain architecture.

The ultimate tensile strength (σ_B) and elongation (ϵ_B) of EPE triblock copolymers can be broadly classified into three categories: weak, intermediate, and strong materials. The ductility and tensile strength increase with molecular weight up to saturation values achieved when $M_n \geq 251$ kDa. Since the ultimate strength of ABA triblock copolymers depends predominantly on the strength of the end blocks, the saturation values of σ_B and ϵ_B reflect the ultimate properties of the linear low-density polyethylene generated from the hydrogenation of 1,4-polybutadiene. Interestingly, samples with high tensile strengths are also those that are microphase separated in the melt, while the samples which undergo crystallization-induced phase segregation have the lowest strengths. Therefore, the tensile strength of EPE may be influenced by the microphase separation mode; however, molecular weight effects on the ultimate mechanical strengths cannot be easily decoupled in the present study. Seguela and Prud'homme[19] have reported similar results: melt-crystallized EPEs exhibited much higher tensile strengths than solution-crystallized ones, since the melt-crystallized EPE undergoes incompatibility-induced microphase separation, whereas the solution-crystallized samples segregate due to crystallization. While the exact factors controlling the correlation between microphase separation mode and tensile behavior are not understood, the microstructural model depicted in Figure 9 provides an enticing opportunity for speculation. Regardless of the phase separation mode, drawing of EPE normal to the interdomain

lamellae results in a low modulus response due to the rubbery P domains. For homopolyethylene, the tensile modulus transverse to the chain axis is weaker than that parallel to the chain axis. Consequently, applied strain along the direction of the lamellar planes for crystallization segregated EPEs results in failure because the strain direction is transverse to the chain axis (Figure 9b). On the other hand, EPEs with incompatibility-induced microphase separation (Figure 9a) form a stronger geometry, since strain applied along the interdomain lamellar planes translates into a strain parallel to the chain axis.

Conclusion

A series of symmetric EPE triblock copolymers with different molecular weights ranging from 27 to 372 kg/mol have been investigated in order to study the effect of microphase separation mode on the solid-state chain microstructure and mechanical properties. The final microstructure depends sensitively on the microphase separation mode. Symmetric EPEs with high molecular weights microphase separate into a lamellar structure before crystallization so that crystallization is geometrically confined within the microdomains. The polyethylene chains in the E crystals are oriented parallel to the planes of interdomain lamellar structure. The observed scaling relationship for the lamellar domain spacing as a function of the degree of polymerization is consistent with existing theoretical predictions by DiMarzio, Guttman, and Hoffman as well as those of Whitemore and Noolandi for semicrystalline amorphous diblock copolymers. In contrast, EPEs with low molecular weights undergo crystallization-induced microphase separation, for which microphase separation is largely controlled by the chain defects due to ethyl branches resulting in a chain-folded lamellar structure for the polyethylene domains similar to that of semicrystalline homopolyethylene. In this case, however, the lamellar domain spacing scales with degree of polymerization as $d \sim N_0^{0.22}$ ($d \sim N_0 N_a^{-0.78}$), in strong disagreement with existing theories. This inconsistency may stem from the formation of solid-state microstructures under crystallization-induced microphase separation that differ from the theoretically assumed equilibrium crystallization behavior. Pinning of both ends of the amorphous P domain to interfaces with the semicrystalline E domains by virtue of the triblock molecular architecture might also affect the final solid-state microstructure. The ultimate tensile strengths of EPE triblock copolymers depend on the mode of microphase separation: crystallization-induced segregation yields materials with lower tensile strengths than those which exhibit templated crystallization within a microphase-separated melt. Microstructural studies have revealed a possible molecular mechanism to explain the observed phenomena.

Acknowledgment. The authors gratefully acknowledge financial support from Medtronic Corporation. Portions of this work were performed at the DuPont−Northwestern−Dow Collaborative Access Team (DND-CAT) Synchrotron Research Center located at Sector 5 of the Advanced Photon Source. Use of the Advanced Photon Source was supported by the U.S. Department of Energy, Basic Energy Sciences, Office of Energy Research, under Contract W-31-109-Eng-38. This research also made extensive use of the NSF-MRSEC supported Institute of Technology Characterization Facility at the University of Minnesota, Twin Cities Campus, under Award DMR-0212302.

References and Notes

(1) Meier, D. J. *Polym. Prepr.* **1974**, 15, 171.
(2) Helfand, E. *Macromolecules* **1975**, *8*, 522.
(3) Helfand, E.; Wasserman, Z. R. *Macromolecules* **1976**, *9*, 879.
(4) Leibler, L. *Macromolecules* **1980**, *13*, 1602.
(5) Matsen, M. W.; Thompson, R. B. *J. Chem. Phys.* **1999**, *111*, 7139.
(6) Mayes, A. M.; Olvera de la Cruz, M. *J. Chem. Phys.* **1989**, *91*, 7228.
(7) Hashimoto, T. *Macromolecules* **1980**, *13*, 1237.
(8) Quiram, D. J.; Register, R. A.; Marchand, G. R. *Macromolecules* **1997**, *30*, 4551.
(9) Nojima, S.; Kato, K.; Yamamot, S.; Ashida, T. *Macromolecules* **1992**, *25*, 2237.
(10) Ryan, A. J.; Hamley, I. W.; Bras, W.; Bates, F. S. *Macromolecules* **1995**, *28*, 3860.
(11) Hamley, I. W.; Fairclough, J. P. A.; Terrill, N. J.; Ryan, A. J.; Lipic, P. M.; Bates, F. S. *Polymer* **1997**, *39*, 1429.
(12) Rangarajan, P.; Register, R. A.; Fetters, L. J. *Macromolecules* **1993**, *26*, 4640.
(13) DiMarzio, E. A.; Guttman, C. M.; Hoffman, J. D. *Macromolecules* **1980**, *13*, 1194.
(14) Whitmore, M. D.; Noolandi, J. *Macromolecules* **1988**, *21*, 1482.
(15) Douzinas, K.; Cohen, R. E.; Halasa, A. F. *Macromolecules* **1991**, *24*, 4457.
(16) Nojima, S.; Yamamoto, S.; Ashida, T. *Polym. J.* **1995**, *27*, 673.
(17) Unger, R.; Beyer, D.; Donth, E. *Polymer* **1991**, *32*, 3305.
(18) Cohen, R. E.; Cheng, P. L.; Douzinas, K.; Kofinas, P.; Berney, C. V. *Macromolecules* **1990**, *23*, 324.
(19) Seguela, R.; Prud'homme, J. *Polymer* **1989**, *30*, 1446.
(20) Holden, G.; Legge, N. R. In *Thermoplastic Elastomers*, 2nd ed.; Hanser Publishers: New York, 1996; pp 48−69.
(21) Quirk, R. P.; Morton, M. In *Thermoplastic Elastomers*, 2nd ed.; Hanser Publishers: New York, 1996; pp 72−100.
(22) Dair, B. J.; Honeker, C. C.; Alward, D. B.; Avgeropoulos, A.; Hadjichristidis, N.; Fetters, L. J.; Capel, M.; Thomas, E. L. *Macromolecules* **1999**, *32*, 8145.
(23) Childers, C. W.; Kraus, G. *Rubber Chem. Technol*. **1967**, *40*, 1183.
(24) Holden, G.; Bishop, E. T.; Legge, N. R. *J. Polym. Sci., Part C* **1969**, *26*, 37.
(25) Beecher, J. F.; Marker, L.; Bradford, R. D.; Aggarwal, S. L. *Polym. Prepr.* **1969**, *8*, 1532.
(26) Honeker, C. C.; Thomas, E. L. *Chem. Mater.* **1996**, *8*, 1702.
(27) Lim, L. S.; Harada, T.; Hillmyer, M. A.; Bates, F. S. *Macromolecules* **2004**, *37*, 5847.
(28) Falk, J. C.; Schlott, R. J. *Macromolecules* **1971**, *4*, 152.
(29) Falk, J. C.; Schlott, R. J. *Angew. Makromol.* **1972**, *21*, 17.
(30) Mohajer, Y.; Wilkes, G. L.; Wang, I. C.; McGrath, J. E. *Polymer* **1982**, *23*. 1523.
(31) Lovinger, A. J.; Han, B. J.; Padden, F. J.; Mirau, P. A. *J. Polym. Sci., Part B: Polym. Phys.* **1993**, *31*, 115.
(32) Hillmyer, M. A.; Bates, F. S. *Macromolecules* **1996**, *29*, 6994.
(33) Ness, J. S.; Brodil, J. C.; Bates, F. S.; Hahn, S. F.; Hucul, D. A.; Hillmyer, M. A. *Macromolecules* **2002**, *35*, 602.
(34) Koppi, K. A. Ph.D. Thesis, University of Minnesota, Minneapolis, 1993.
(35) Hermel, T. J.; Wu, L.; Hahn, S. F.; Chaffin, K. A.; Gerberich, W. W.; Bates, F. S. *Macromolecules* **2003**, *36*, 2190.
(36) Brandrup, J., Immergut, E. H. Eds. *Polymer Handbook*, 3rd ed.; Wiley: New York, 1989.
(37) Bates, F. S.; Schulz, M. F.; Rosedale, J. H.; Almdal, K. *Macromolecules* **1992**, *25*, 5547.
(38) Rosedale, F. H.; Bates, F. S. *Macromolecules* **1990**, *23*, 2329.
(39) Douzinas, K.; Cohen, R. E. *Macromolecules* **1992**, *25*, 5030.
(40) Kofinas, P.; Cohen, R. E. *Macromolecules* **1994**, *27*, 3002.

MA0501794